Desalination and Water Treatment
www.deswater.com

doi:10.5004/dwt.2019.24501

165 (2019) 232–243
October

Production of KOH-activated carbon from date press cake: effect of the activating agent on its properties and Pb(II) adsorption potential

Zoha Heidarinejad[a,b], Omid Rahmanian[b], Mohsen Heidari[b,*]

[a]*Food Health Research Center, Hormozgan University of Medical Sciences, Bandar Abbas, Iran, email: z_heidarinejad@yahoo.com (Z. Heidarinejad)*
[b]*Department of Environmental Health Engineering, Faculty of Health, Hormozgan University of Medical Sciences, Bandar Abbas, Iran, email: om.rahmanian@gmail.com (O. Rahmanian), moheidari84@gmail.com (M. Heidari)*

Received 9 October 2018; Accepted 5 June 2019

ABSTRACT

The aim of this study was to evaluate the efficiency of KOH-activated carbon derived from date press cake (DPC) for the adsorption of Pb(II) from aqueous solutions. Raw DPC was first converted into a carbonized material (CM) and then activated at dry KOH:CM weight ratios of 1:1 (AC1) and 4:1 (AC4). The adsorbents were characterized using FTIR, FESEM-EDX, BET and Boehm titration method. AC1 and AC4 showed microporous structure with BET surface areas of 1237.2 and 2938.7 m^2 g^{-1}, respectively. The prepared activated carbons (ACs) successfully adsorbed Pb(II) from aqueous solution with maximum monolayer adsorption capacities of 59.0 mg g^{-1} (AC1) and 101.3 mg g^{-1} (AC4). The adsorption of Pb(II) onto both ACs was well described by Elovich and pseudo-second order kinetic models, indicating that the rate of Pb(II) adsorption onto the ACs was mainly controlled by chemical adsorption. Isotherm study showed that the adsorption of Pb(II) onto AC1 took place in multilayer on a heterogeneous surface, while the Pb(II)/AC4 adsorption process occurred in a monomolecular layer with a homogenous distribution among the adsorption sites at different energies. This study showed that AC4 has a high specific surface area and successfully adsorbs Pb(II) even from saline aqueous solutions.

Keywords: Adsorption; Activated carbon; Date press cake; Pb (II)

1. Introduction

Heavy metal pollution of aquatic ecosystems is a crucial environmental problem [1]. Lead is among the high priority heavy metals and its toxic effect on human health is well-known documented [2]. Anthropogenic sources and uses of lead, through which it can be introduced into the environment, are activities related to alloys, pigments, antiknock agents, glassware, ceramics, plastic, tetramethyl lead, lead-acid batteries, cable sheathings, solder, and pipes or tubing [3].

The presence of Pb(II) in water may cause serious damage to the liver, kidney, nervous system, reproductive system; reduce hemoglobin formation; and cause infertility and abnormalities in pregnant women [4,5]. Therefore, it is necessary to treat wastewater containing Pb(II) before being discharged into water streams for the protection of the environment and public health.

The commonly used treatment methods for removing Pb(II) from wastewater are adsorption, chemical precipitation, electrodialysis, photocatalysis, and membrane processes [1,6]. Among them, adsorption process on activated carbon is known as an effective and simple method for the removal of heavy metals from aqueous solutions [7,8]. This adsorbent has highly porous structure with high surface reactivity and large surface area [9].

Large-scale application of commercial activated carbon may be problematic if this material be prepared from expensive and nonrenewable precursors. Therefore, in

*Corresponding author.

recent years, the focus of researches has been directed into the production of activated carbon from cheap and renewable precursors [9,10]. In this regards, some researches have focused on Pb(II) removal from aqueous solutions using activated carbons prepared from abundant agricultural biomass such as cherry kernels [11], palm oil mill effluent [12], lemon peel [13], tamarind wood [14] and Cucumis melo peel [15].

Date palm Phoenix dactylifera is a subtropical and tropical tree, which is cultivated in 30 countries [16]. According to FAO report, the worldwide amount of date fruit production was around 8.5 million tons in 2016 [17]. In date processing industries, various products including date pastes, date juice concentrates, and fermented date products (organic acids, vinegar and alcohol) are produced from date fruits [16]. In such industries, a major portion of date fruit, i.e. Date Press Cake (DPC), is remained on filter presses after extracting its liquid products [18,19]. In Iran, in which around 1.16 million tons date fruit was produced in 2016 [17], a huge amount of DPC is generated daily and mainly dumped into open lands and drains [19].

Up to date, numerous studies have been done on the preparation of activated carbon from different parts of the palm tree including palm kernel shell [20,21], date palm leaflets [22,23] and date palm fibers [24,25]. However, limited studies have focused on the conversion of DPC into activated carbon [19,26]. To the best of our knowledge, the activated carbon prepared from DPC has not been used for the adsorption of Pb(II) from aqueous solutions.

According to literature, initial carbonization of organic precursors improves their porosity and facilitates the penetration of activating agent into the carbonized material of char structure during final chemical activation [27]. On the other hand, the unstable structure of raw DPC with pulpy structure in aqueous solution troubles with its chemical activation through impregnation method. Therefore, in this study, raw DPC was converted into activated carbon through a two-stage dry chemical activation procedure; carbonization and physical mixing of carbonized material with various amounts of dry KOH. The main aim of this study was to evaluate the efficiency of the KOH-activated carbon derived from DPC for the adsorption of Pb(II) from aqueous solution. The kinetics and isotherms of Pb(II) adsorption onto the ACs were analyzed by non-linear form of the kinetic and isotherm models. The main morphological, textural and chemical characterizations of the ACs were also analyzed.

2. Material and methods

2.1. Chemicals and materials

Lead nitrate (≥99.9% purity), potassium hydroxide (≥99.0% purity), hydrochloric acid (≥37% purity), Sodium hydroxide (≥99.0% purity), sodium hydrogen carbonate (≥99.0% purity) and sodium carbonate (≥ 98.0% purity) were purchased from Merck Co., Germany. Initially, a Pb(II) stock solution (1000 mg L^{-1}) was prepared from lead nitrate, then working solutions were obtained from the stock solution. Raw DPC, a pasty material, was obtained from a local date fruit processing industry.

2.2. Preparation of activated carbon

Raw DPC was first dried at 110°C and its particle size was reduced to less than 1 mm. Pretests showed that a significant amount of raw DPC (mainly soluble fraction) was lost during its direct impregnation with KOH solution. In this regard, activated carbon was prepared through a two-step procedure, i.e. initial carbonization and chemical activation with NaOH pellets under dry conditions. First, the dried DPC was placed in a horizontal stainless steel reactor and heated up to 500°C in a furnace at a rate of 20°C min^{-1} and kept at this temperature for 2 h. The obtained carbonized material (CM) was then physically mixed with KOH pellets at KOH:CM weight ratios of 1:1 and 4:1.

The mixture of KOH and CM was placed into a stainless steel reactor and heated up to 750°C at the rate of 20°C min^{-1} and kept at this condition for 1.5 h. Carbonization, chemical activation and cooling stages were performed under the nitrogen flow of 100 cm^3 min^{-1}.

After activation, the prepared activated carbon was separated from alkaline material through repeatedly washing the mixture with deionized water and dilute HCl (0.1 M) on a filter until the filtrate pH became neutral. Finally, the obtained activated carbon samples were dried in oven at 110ºC for 24 h. The activated carbons prepared at KOH:CM weight ratios of 1:1 and 4:1 were labeled as AC1 and AC4, respectively, and used in Pb(II) adsorption experiments.

The yields of carbonized material and activated carbon production from raw DPC were determined as:

$$Yield(\%) = \frac{W_C}{W_R} \times 100 \quad (1)$$

where W_C and W_R are dry weights of products (CM or ACs) and raw DPC (g), respectively.

2.3. Adsorbent characterization

Textural properties of AC1 and AC4 were analyzed by N_2 adsorption-desorption at 77 K using a surface area analyzer (Belsorp-mini II, BEL Japan Inc., Osaka, Japan). The specific surface area or S_{BET} of the ACs was determined by Brunauer-Emmett-Teller (BET) equation. Total pore volume (V_T) of ACs was determined as the maximum amount of nitrogen which adsorbed at the relative pressure (P/P^0) of 0.99 [28]. Micropore volume was determined through t-plot according to IUPAC [29] and the mesopore volume (V_m) was calculated as the difference between total and micropore volumes [30]. The average pore diameter (D) was calculated from the relation $D = 4V_T/S_{BET}$ [31].

The morphology and elemental composition of AC1 and AC4 were analyzed by a field emission scanning electron microscope equipped with a dispersive X-ray spectrometer (FESEM-EDX, Tescan Mira 3 LMU).

The functional groups present on the surfaces of AC1 and AC4 were ascertained by a Fourier Transform Infrared Spectroscopy (FT-IR) Nicolet Avatar 360 (Nicolet, USA). The FT-IR spectra of the materials, with 4 cm^{-1} resolution and 20 scans min^{-1}, were recorded between 4000–400 cm^{-1} through potassium bromide (KBr) pellet method.

Additionally, the chemical characteristics of AC1 and AC4 surfaces were analyzed by Boehm titration method

[32,33]. The point of zero charge pH (pH_{PZC}) of the ACs was determined by pH drift method as proposed by Liu et al. [34].

2.4. Adsorption experiments

Batch Adsorption experiments were carried out by taking 25 ml of Pb(II) solution into 50 ml flasks. All experiments were done at a shaking rate of 250 rpm under room temperature (298±0.5 K).

The effect of solution pH (2–7) on Pb(II) adsorption was evaluated with initial Pb(II) concentration of 100 mg L^{-1} at 120 min contact time. The kinetics of Pb(II) adsorption on the ACs were analyzed at contact times ranged from 2.5 to 120 min with initial Pb(II) concentration of 100 mg L^{-1} and the selected pH value. Isotherm study was carried out under the following conditions: initial Pb(II) concentrations ranged from 5 to 200 mg Pb L^{-1}, equilibrium contact time and selected pH value.

The effect of ionic strength on the adsorption system was evaluated with deionized water containing 200 mg L^{-1} and various molar NaCl concentrations (0–1 M) at equilibrium contact time and selected pH value. In all experiments, the pH of solutions was adjusted by dilute HCl or NaOH and measured with a pH meter (WTW, Germany).

At the end of each run, the solutions were filtered and the residual concentration of Pb(II) was measured by atomic absorption spectroscopy (Younglin AAS 8020, South Korea). All calibration and sample solutions were acidified before measuring their Pb(II) content.

The capacities of ACs for the adsorption of Pb(II) at equilibrium condition (q_e) and at time t (q_t) were calculated as follows:

$$q_e = \frac{(C_i - C_e)V}{W} \tag{2}$$

$$q_t = \frac{(C_i - C_t)V}{W} \tag{3}$$

where C_i, C_e and C_t are the initial, equilibrium and at time t of Pb(II) concentrations (mg Pb L^{-1}), respectively, V is the volume of suspension (L), and W is the dry weight of the ACs in suspension (g).

2.5. Data analysis

Five common kinetic models including pseudo-first order, pseudo-second order, Elovich, intraparticle diffusion and Boyd's were used for the kinetics of Pb(II) adsorption onto the ACs. Moreover, four isotherm models, namely Freundlich, Langmuir, Redlich-Peterson, and Temkin, were used to analyze the experimental Pb (II) equilibrium adsorption data (Table S1). The non-linear forms of all isotherm models and kinetic models, except intraparticle diffusion and Boyd models, were fitted to the experimental adsorption data using OriginLab Pro (2018) software. Finally, the best-fitted kinetic and isotherm models were identified by the coefficient of determination (R^2) and average relative error (ARE) (Table S2).

3. Results and discussion

3.1. Yield and textural characterization of the material

The yield of CM preparation from raw DPC was 45.5%, while the yield values for AC1 and AC4 were 30.94% and 22.47%, respectively. These values are comparable to those reported for some KOH-activated carbons derived from agro-industrial wastes reported in the literature [35–37].

The decrease in AC1 yield compared to that of CM could be related to the intercalation of K into the CM structure and its subsequent elimination and dehydration reactions [38]. Such phenomena probably resulted in further decrease in yield of AC prepared with KOH:CM weight ratio of 4:1.

The N_2 adsorption/desorption isotherms and the pore size distribution of AC1 and AC4 are shown in Fig. 1. According to IUPAC (International Union of Pure and Applied Chemistry) classification, the isotherm profile obtained for AC1 and AC4 could be classified as type I (b), which is characteristic of microporous materials having pore size distributions over a broad range including wide micropores and possibly narrow mesopores [29]. Such microporous feature of ACs is reflected in pore size distribution plot, which indicates that the most of pores had sizes smaller than 2 nm (Fig. 1b, c). As shown in Table 1, the S_{BET} of AC4 (2938.7 m^2 g^{-1}) was higher than that of AC1 (1237.2 m^2 g^{-1}). Nieto-Márquez et al. [39] and Muniandy et al. [40] also reported that the S_{BET} of activated carbons prepared from waste tire and rice husk, respectively, was increased by applying higher KOH:CM weight ratios. Therefore, heating of CM in the presence of higher amount of activating agent promoted the surface area of AC. Accordingly, the V_T of AC4 was far higher than that of AC1. The higher S_{BET} and V_T of AC4 could be related to the more intercalation of the alkaline metal into the carbon structure in the presence of higher amount of KOH. However, the microporosity of AC was decreased when CM was activated at higher KOH:CM ratio, which indicates that the spaces between atomic layers of carbon were widen in the presence of more activating agent [31,40]. Considering the S_{BET} of CM (3.47 m^2 g^{-1}), a micro-mesoporous activated carbon with high specific surface area (2938.7 m^2 g^{-1}) could be produced by KOH-activating of DPC under dry conditions. The activation mechanism with KOH is in accordance with the following main reactions [41]:

$$6KOH + 2C \rightarrow 2K + 3H_2 + 2K_2CO_3 \tag{4}$$

$$2KOH + 2C \rightarrow 2K + 2CO + H_2 \tag{5}$$

The KOH penetration into the carbon structure, followed by burn-off of carbon bonds and release of gaseous products probably are the main causes of the porosity development.

FESEM images of AC1 and AC4 are presented in Fig. 2. As can be seen, the surface alteration and porosity were more pronounced in AC4.

The EDX analysis results for the elemental composition of CM and ACs are shown in Table 2. As can be seen, carbon is the main elements constituting the CM and ACs. In addition, the K content of the ACs was less than that of CM the negligible amount of K in the activated carbons indicating the efficient removal of the remaining KOH

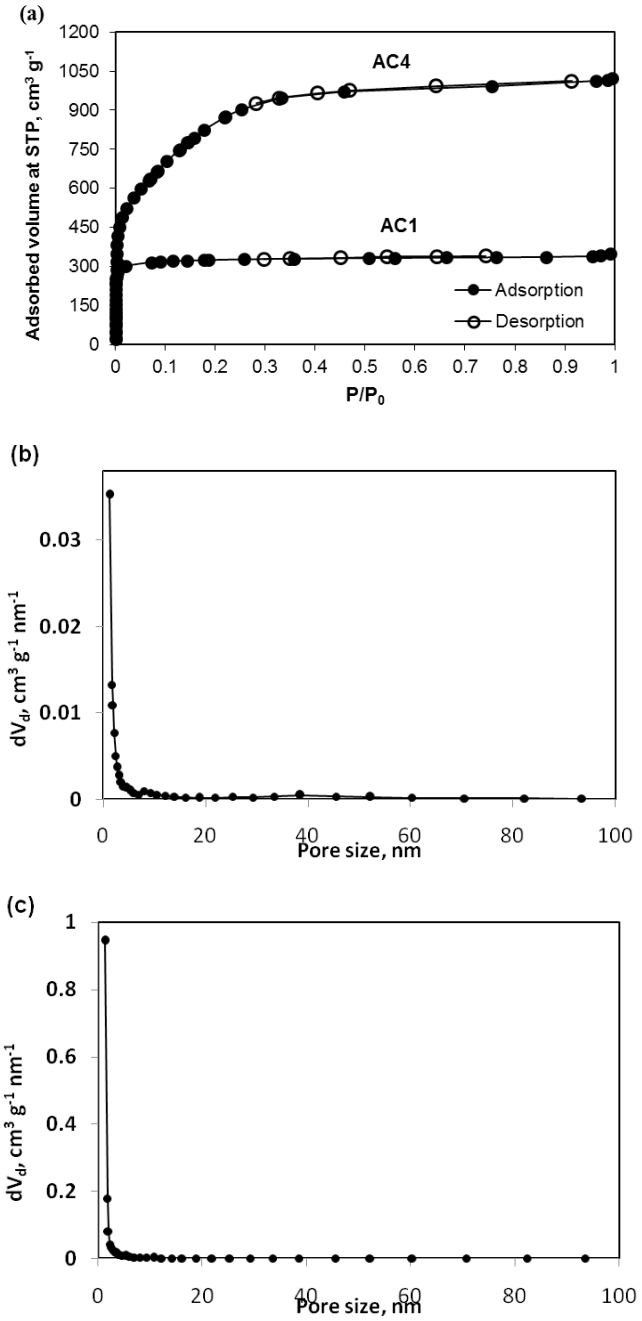

Fig. 1. (a) N_2 adsorption/desorption isotherms at 77 K, and pore size distribution of (b) AC1 and (c) AC4.

during the washing step. Overall, the higher content of carbon in ACs indicates the more purity of the ACs compared to CM.

3.2. Chemical surface characterization

FT-IR spectroscopy was used to identify the main characteristics functional groups present on the AC1 and AC4 surfaces (Fig. 3). According to AC1 spectrum, the band at 3436 cm^{-1} is attributed to –OH functional group,including hydrogen interactions. The band located at around 2855 cm^{-1} corresponds to C-H stretching vibration. The peak appeared at 1722 cm^{-1} can be assigned to C=O axial deformation of aldehyde, lactone, ketone and carboxyl groups. The spectrum peaked at 1086 cm^{-1} is attributed to C-O such as that in alcohols, phenols, acids, ethers or esters. The band at 476 cm^{-1} is the characteristic of the vibrational mode of C-N-C group. Compared to the AC1 spectrum, some changes can be noted in the position and intensity of some peaks in the AC4 spectrum. As shown in Fig. 3, the position of peaks related to –OH, C-H, C-C, C-O and C-N-C were at 3440, 2922, 1431, 1086 and 473 cm^{-1} in AC4 spectrum.

Table 1
Textural characteristics of the activated carbons

Parameters	AC1	AC4
S_{BET}	1237.2 $m^2 g^{-1}$	2938.7 $m^2 g^{-1}$
Pore diameter	1.74 nm	2.15 nm
Total pore volume	0.5398 $cm^3 g^{-1}$	1.578 $cm^3 g^{-1}$
Micropore volume	0.487 $cm^3 g^{-1}$	1.240 $cm^3 g^{-1}$
Micropore percentage	90.14%	78.6%
Mesopore volume	0.053 $cm^3 g^{-1}$	0.338 $cm^3 g^{-1}$
Mesopore percentage	9.85%	21.39%

Oxygen functional groups present on the adsorbent surface significantly contribute in adsorption process because they act as active sites which are capable to attract adsorbate molecules [28]. Boehm titration method was used to quantify the oxygen functional groups present on the ACs. It was found that the amounts of acid functional groups in AC1 and AC4 were 0.38 and 1.01 mmol g^{-1}, respectively. Therefore, activation with higher amount of KOH increased the content of acid functional groups in the prepared activated carbon. The higher content of oxygen-containing (acidic functional) groups in AC4 compared to AC1 is in accordance to the higher oxygen content of AC4 (Table 2).

3.3. Effect of pH on Pb(II) adsorption

The chemistry of adsorbate in aqueous solution and the ionic state of functional groups on the adsorbent surface depends on the solution pH [42]. The experiments for the effect of initial pH on the adsorption of Pb(II) were done at solution pH ranged from 2 to 7 and the results are presented in Fig. 4. As can be seen from the figure, the RE of Pb(II) onto both ACs was negligible at pH 2 and increased to 68.58% (AC1) and 95.0% (AC4) at pH 6 (final pH = 5.97).

At acidic pH, H^+ ions compete with cationic metal ions to adsorb on the adsorbent surface. Therefore, the inhibitory effect of H^+ ions on the adsorption of Pb(II) would be decreased with the increase in solution pH [43]. As is known, the ACs surfaces acquired positive charge at pH < pH_{PZC} (pH_{PZC} > 6 for both ACs) and negative charge at pH > pH_{PZC} [44]. Therefore, the net charge on both ACs was positive for the pH values ranged from 2 to 6. In this condition, the repulsive interaction between Pb(II) and ACs surface probably was increased at more acidic conditions, further decreasing the amount of Pb(II) adsorption [45,46].

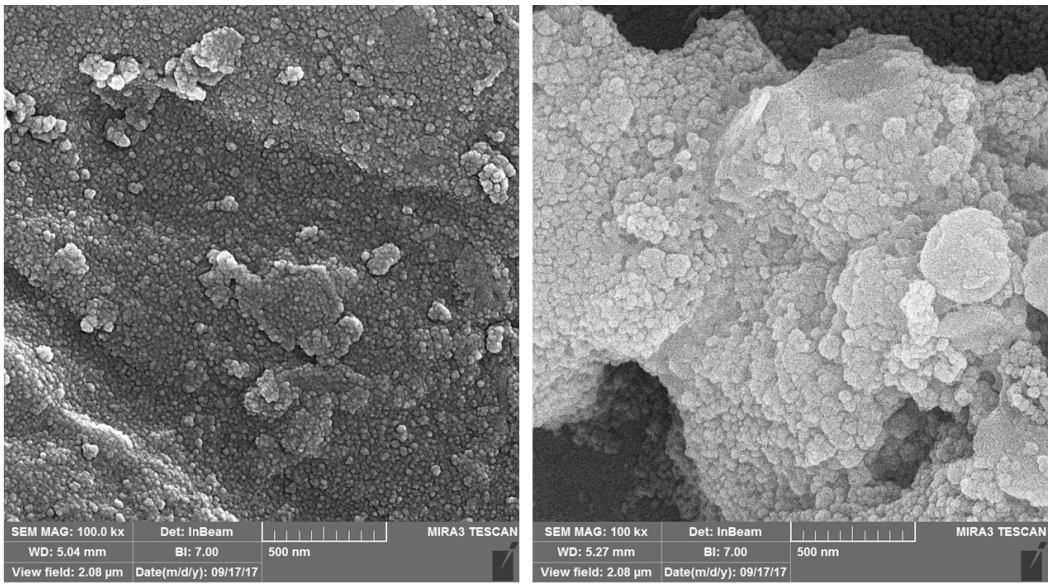

Fig. 2. FESEM images of AC1 (left) and AC4 (right).

Table 2
Elemental composition of CM and ACs based on EDX analysis (%)

Element	CM	AC1	AC4
C	62.48	75.10	74.51
N	5.90	6.89	6.83
O	16.95	15.04	17.44
Na	1.68	–[a]	–
Mg	1.10	–	0.43
P	0.44	0.55	0.09
S	1.61	0.55	0.27
Cl	3.14	–	–
K	6.57	1.72	–
Cr	0.13	0.14	0.43
Total	100	100	100

[a]not detected

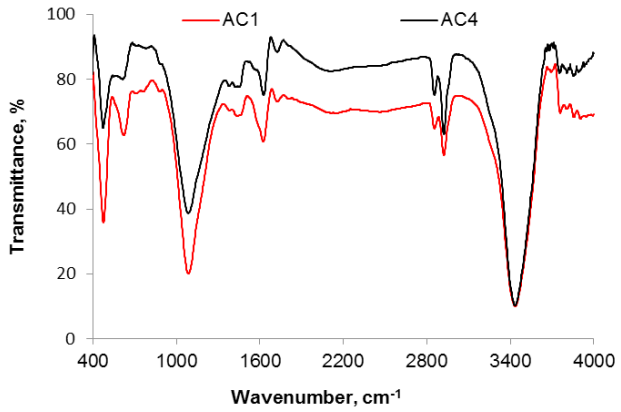

Fig. 3. FT-IR analysis of AC1 and AC4.

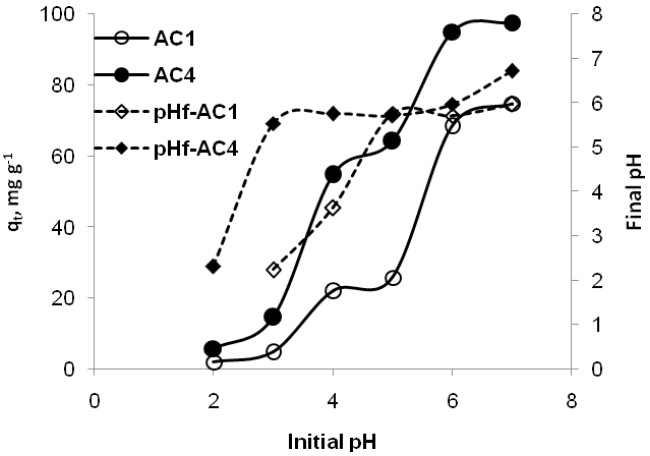

Fig. 4. Pb(II) removal efficiency as a function of initial pH (C_0 = 100 mg L^{-1}, adsorbent dose = 1 g L^{-1}, contact time = 120 min).

It should be noted that the distribution of Pb(II) species in aqueous solution is a function of the pH of the solution. In general, the reaction of hydrolysis of lead ions is as follows:

$$Pb^{+2} + 2nH_2O \rightleftarrows Pb(OH)^{2-n}_{n} + nH_3O^{+} \quad (6)$$

where n is changed at various pH values [47]. The main species of lead in pH values greater than 7 are mainly low soluble hydroxides [48]. Therefore, the precipitation of a portion of lead hydroxide may start at pH values above 7 [49]. In this regard, in accordance to the numerous studies on the adsorption of Pb(II) from aqueous solution (Table 3), pH of 6 was selected for subsequent experiments in order to confirm that no hydroxide precipitation occurred during the adsorption process. It must be noted that the pH of the solutions with initial pH of 6 did not increase at the end of experiment.

Table 3
Comparison of maximum monolayer adsorption capacity (q_m) of Pb(II) onto various biomass-derived activated carbons

Precursor	Activating agent	BET surface area ($m^2 g^{-1}$)	Optimum pH	q_m (mg g^{-1})	Equilibrium time	Reference
Cherry kernel	H_3PO_4	657.1	6	180.30	30 min	[11]
Palm oil mill effluent	H_3PO_4	59.2	5.5	94.34	50 min	[12]
Sea-buckthorn stones	$ZnCl_2$	829	6	25.29	15 min	[65]
Persian mesquite grain	H_3PO_4	1243	5	384.00	40 min	[66]
Olive Stones	KOH	1280.7	5	23.47	180 min	[67]
Date Press Cake	KOH	1237.2 (AC1)	6	58.96	45 min	Present study
		2938.7 (AC4)		101.28		

3.4. Adsorption kinetics

Contact time is an inevitable parameter during mass transfer stage in adsorption process. The effect of contact time on the adsorption of Pb(II) onto AC1 and AC4 was studied with initial Pb(II) concentration of 100 mg L^{-1}, adsorbate dose of 1 g L^{-1} and pH of 6. As shown in Fig. 5, it is clear that the rate of Pb(II) adsorption was rapidly increased in the beginning and gradually increased until equilibrium was reached. At the beginning of adsorption process, the concentration of Pb(II) ions in solution (as driving force) was high and all of active sites on the adsorbent surface were vacant. After a given time (around 45 min), the reduced amounts of Pb(II) ions and vacant surface active sites probably led to negligible increase in Pb(II) uptake with time.

Adsorption kinetic studies are very important for understanding the order of reaction rate and the dynamics of the adsorption reaction [50]. In order to find the best kinetic model describing the adsorption of Pb(II) onto AC1 and AC4, the kinetic models of pseudo-first order [51], pseudo-second order [52] and Elovich [53] were nonlinearly fitted to experimental data (Fig. 5).

The magnitude of R^2 and ARE values listed in Table 4 indicate that the adsorption of Pb(II) onto the ACs were well fitted by pseudo-second order and Elovich models. The Elovich model assumes that the interactions between adsorbate molecules on the adsorbent surface are not influenced by adsorption kinetics at low surface coverage. It also assumes that the surface of adsorbent is energetically heterogeneous [54]. The pseudo-second order model assumes that the sorption process involves a chemical reaction. It also assumes the proportional relationship between sorption capacity and number of active sites on the sorbent [55]. In this regard, the adsorption of Pb(II) onto both ACs occurred predominantly by chemisorption.

The kinetic constants of h_0 and α are indicative of initial adsorption rate. According to Table 4, the values of these constants for the adsorption of Pb(II) onto AC4 were higher than those obtained for Pb(II)/AC1 system. Therefore, it seems that the higher S_{BET} provided more vacant sites at the beginning of adsorption process compared to that of AC1.

The intraparticle diffusion model proposed by Weber and Morris [56] was applied in order to understand how the diffusion of Pb(II) molecules onto AC1 and AC4 takes place. This model assumes that the adsorption process occurs in three stages including mass transfer to the external surface of the sorbent, mass transfer to the sorbent internal surface, and then adsorption of adsorbate molecules onto active adsorbent sites [57].

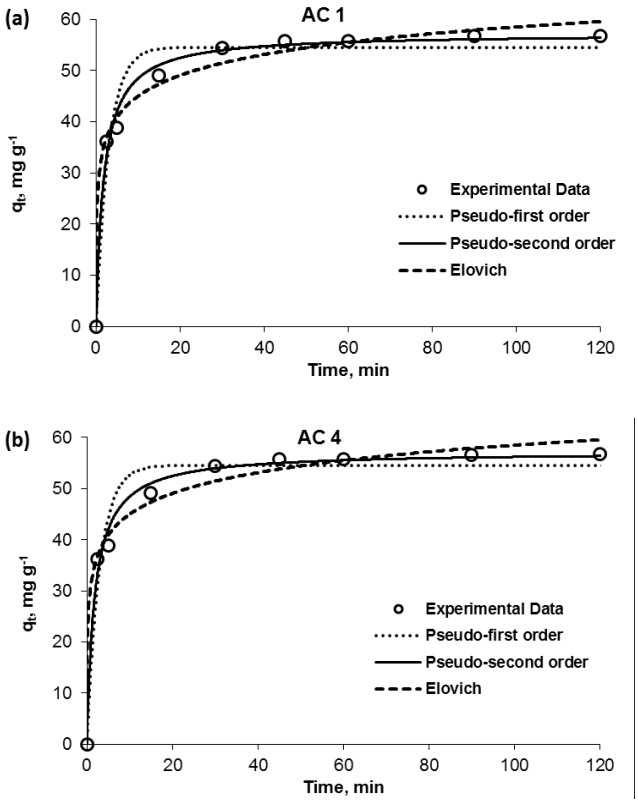

Fig. 5. Non-linear adjustments of the kinetic models with the experimental data of Pb(II) adsorption (C_0 = 100 mg L^{-1}, pH = 6, adsorbent dose = 1 g L^{-1}).

The values of intraparticle diffusion constants, k_{id} and C_i, were determined through plotting q_t vs. $t^{0.5}$ (Fig. 6a). k_{id} and C_i represent intraparticle diffusion rate constant (mg g^{-1} $min^{-0.5}$) and the thickness of boundary layer (mg g^{-1}), respectively. As seen from Fig. 6a, the data points do not fall on a straight line, but they could be aligned in two distinct linear stages. The first sharper stage is related to the instantaneous adsorption of Pb(II) molecules, and the second stage is attributed to the intraparticle diffusion of Pb(II)

Table 4
Parameters of the kinetic models for the adsorption of Pb(II) onto AC1 and AC4

Parameters	AC1	AC4
Pseudo-first order		
q_e (mg g^{-1})	54.54	91.43
k_1 (min^{-1})	0.3352	0.7192
h_0 (mg g^{-1} min^{-1})	18.287	65.762
R^2	0.960	0.987
ARE	6.40	3.04
Pseudo-second order		
q_e (mg g^{-1})	57.201	93.425
k_2 (min^{-1})	0.0096	0.0198
h_0 (mg g^{-1} min^{-1})	31.607	173.43
R^2	0.9899	0.9970
ARE	3.10	1.40
Elovich		
α (mg g^{-1} min^{-1})	1257.65	3414.11
β (g mg^{-1})	0.1704	0.24035
R^2	0.9876	0.9977
ARE	3.40	1.37

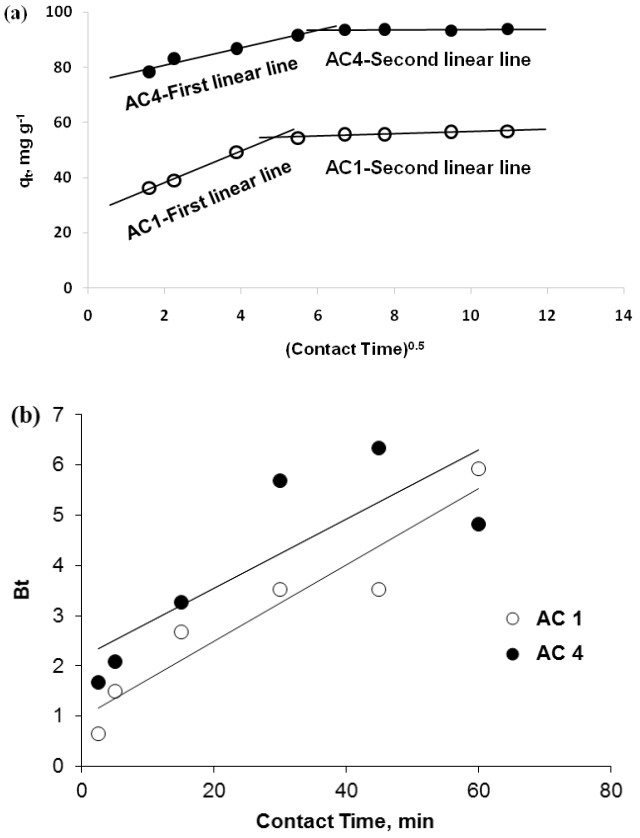

Fig. 6. (a) Intraparticle diffusion and (b) Boyd's plots for the adsorption of Pb(II) onto ACs.

molecules through the pores of the ACs. The intercept of the first stage plots, C_i, gives an insight into the tendency of the adsorbate to be adsorbed on the adsorbent or remain in solution [24]. According to Table 5, the value of C_1 was greater in Pb(II)/AC4 system (77.6 mg g^{-1}) compared to that of Pb(II)/AC1 system (40.2 mg g^{-1}), depicting higher tendency of AC4 surface to the Pb(II) ions than AC1. As shown in Fig. 6, the linear lines did not pass through the origin, suggesting that the intraparticle diffusion was not the only limiting mechanism in the adsorption process.

The Boyd model [58] is used to identify the limiting step of speed between film diffusion and intraparticle diffusion. If Boyd's plot (Bt versus time) is linear and passes from the origin of the coordinates, intraparticle diffusion is the only limiting factor in the adsorption process, but nonetheless, the liquid film diffusion controls the process [59].

As shown in Fig. 6b, although the Boyd plots for the adsorption of Pb(II) onto both ACs present some linearity, but they do not pass through the origin. Therefore, the adsorption rate of Pb(II) onto both ACs were mainly controlled by the film diffusion or chemical reaction.

3.5 Adsorption isotherm

Adsorption isotherms are mathematical relations that are useful for understanding how the adsorbate molecules are partitioned between the aqueous and solid phases under equilibrium condition [26].

In order to analyze the adsorption isotherm of Pb(II) on AC1 and AC4, the nonlinear forms of Freundlich, Langmuir, Redlich-Peterson and Temkin models were fitted to the equilibrium adsorption data (Fig. 7).

The Freundlich isotherm assumes multilayer adsorption onto heterogeneous surfaces, while Langmuir isotherm describe monolayer adsorption (the adsorbed layer is one molecule in thickness) onto homogenous surfaces [60,61]. The Redlich-Peterson isotherm is a hybrid isotherm, in which both Freundlich and Langmuir features are combined [62]. Temkin model assumes that the adsorption heat increases linearly with the coverage of adsorbent [63].

The values of R^2 and ARE presented in Table 6 imply that the adsorption of Pb(II) onto AC1 was well described by Temkin and Redlich-Peterson models. On the other hand, Redlich-Peterson model well described the experimental data of Pb(II) adsorption on AC4. Redlich-Peterson model is generally applied to show the adsorption equilibrium in a wide range of adsorbate concentrations in homogeneous and heterogeneous systems according to their compatibility [64]. If g = 0, the Redlich-Peterson equation behaves as Henry's law, while it will behave according to the Langmuir isotherm when the value of g tends to 1. On the other hand, If g < 1 and the values of a_{RP} and b_{RP} parameters be far higher than 1, Redlich-Peterson equation converges to Freundlich approach [19,64]. With respect to the values of g, a_{RP} and b_{RP} presented in Table 7 for Pb(II)/AC1 adsorption system, the Redlich-Peterson model more likely behaved as Freundlich approach than Langmuir approach. Moreover, the values of R^2/ARE imply that the adsorption of Pb(II) onto AC1 best described by Temkin isotherm model. Therefore, the well description of Pb(II)/AC1 isotherm and kinetic data with Temkin/Freundlich and Elovich models, respectively, indicates that the adsorption of Pb(II) onto AC1 was a mul-

Table 5
Parameters of intraparticle diffusion kinetic for adsorption of Pb(II) onto AC1 and AC4

Parameters	First linear line		Second linear line	
	k_1 (mg g^{-1} min$^{-0.5}$)	C_1 (mg g^{-1})	k_2 (mg g^{-1} min$^{-0.5}$)	C_2 (mg g^{-1})
AC1	5.75	26.63	0.41	52.58
AC4	3.17	74.46	0.01	93.47

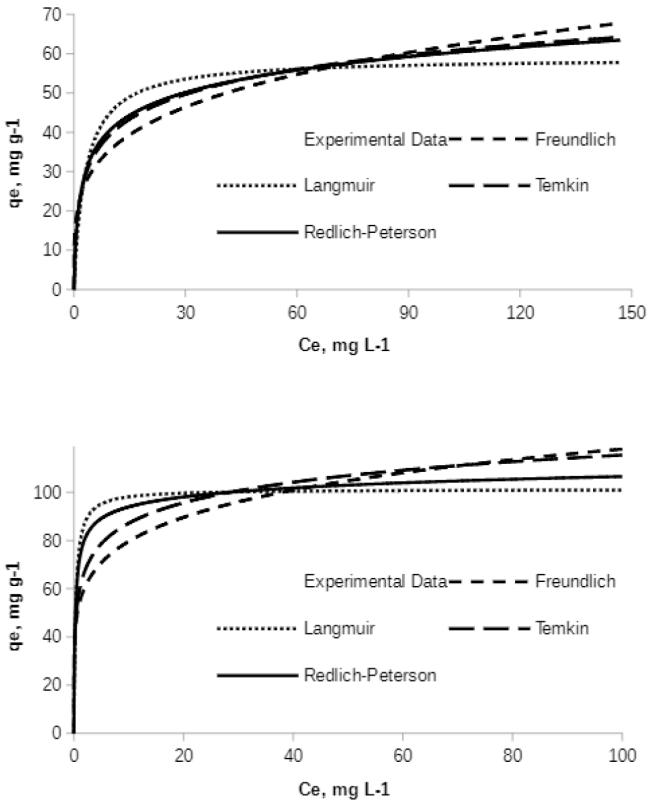

Fig. 7. Non-linear adjustments of the isotherm models with the experimental data of Pb(II) adsorption (C_0 = 5–150 mg L^{-1}, pH = 6, adsorbent dose = 1 g L^{-1}).

tilayer sorption, and the adsorption took place on a heterogeneous surface.

With respect to the g value (≈1) and the values of R^2/ARE for isotherm models (Table 6), it can be concluded that the Langmuir model well described Pb(II)/AC4 adsorption system. On the other hand, as noted previously, the kinetic data of Pb(II)/AC4 adsorption were well fitted with Elovich model. Therefore, it seems that the Pb(II)/AC4 adsorption process occurred in a monomolecular layer with a homogenous distribution among the adsorption sites at different energies.

The separation factor (R_L), in the Langmuir model, was used to determine if the adsorption process is favorable ($0 < R_L < 1$), linear ($R_L = 1$), or unfavorable ($R_L > 1$) [40]. For the range of applied initial Pb(II) concentrations (5–200 mg L^{-1}), the R_L values decreased from 0.3784 to 0.0149 for Pb(II)/AC1 system and from 0.0599 to 0.0015 for Pb(II)/AC4 system, indicating the favorability of Pb(II) adsorption onto the ACs in the concentration range studied.

Table 6
Parameters of isotherm models for the adsorption of Pb(II) onto AC1 and AC4

Parameters	AC1	AC4
Freudlich		
k_F (mg g^{-1})	20.646	53.758
n_F	4.199	5.858
$1/n_F$	0.238	0.170
R^2	0.961	0.883
ARE	15.15	42.97
Langmuir		
q_m (mg g^{-1})	58.96	101.28
k_L (L mg^{-1})	0.328	3.135
R^2	0.964	0.986
ARE	10.44	3.89
Redlich-Peterson		
a_{RP} (L mg^{-1})$^{-g}$	39.730	414.55
b_{RP} (L g^{-1})	1.174	4.790
g	0.871	0.954
R^2	0.992	0.995
ARE	5.92	6.43
Temkin		
k_T (L g^{-1})	7.557	119.79
b_T (J mol^{-1})	9.155	12.297
R^2	0.994	0.958
ARE	5.71	20.59

The maximum monolayer adsorption capacities (q_m) for AC1 and AC4 were 58.96 and 101.28 mg g^{-1}, respectively, which are considerable compared to those reported for several biomass-derived ACs applied for Pb(II) adsorption (Table 3). The isotherm study showed that Pb(II) was more favorably adsorbed onto AC4 than that of AC1. Therefore, AC4 showed better potential for the adsorption of Pb(II) probably due to higher specific surface area, higher pore volume and higher content of oxygen functional groups. Moreover, the proportion of mesopores in AC4 (21.39%) was higher than that of AC1 (9.85%) (Table 1). It is well known that the presence of mesopores may facilitate the transfer of heavy metal ions like Pb(II) within the sorbent structure [68].

3.6. Effect of ionic strength on Pb(II) adsorption

Wastewater from many industries such as textile dyeing, leather tanning, plating and so often contains various levels of ionic strength due to presence of salts like sodium chloride. The ionic strength of aqueous solution may affect the adsorption of metals [69].

The effect of solution ionic strength on the adsorption system was tested with deionized water containing various molar concentrations of NaCl (up to 1 mol). As can be seen from Fig. 8, the fluctuation in the rate of Pb(II) adsorption

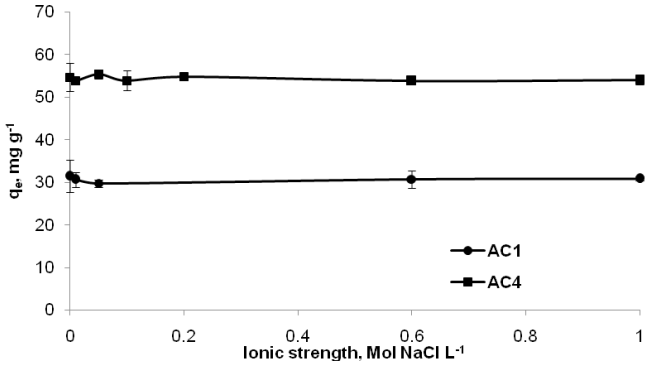

Fig. 8. Effect of ionic strength on Pb(II) adsorption onto ACs (C_0 = 200 mg L^{-1}, pH = 6, adsorbent dose = 1 g L^{-1}).

from aqueous solutions with various ionic strengths was negligible (<2 mg g^{-1} for both ACs). Abdulkarim et al. [70] also reported the negligible effect of ionic strength originated from NaCl on the adsorption of Pb(II) onto the activated carbon produced from Date Pits. It is well known that the outer-sphere surface complexation is significantly influenced by the changes in ionic strength of aqueous solution, while inner-sphere surface complexation between adsorbate and adsorbent surface is ionic strength independent [71]. Therefore, the insensitivity of Pb(II)/ACs system to ionic strength is an indicative of inner-sphere surface complexation, in which Pb(II) formed in-plane covalent bonds with the ACs surfaces [72]. Then, it seems that the electrostatic attraction had negligible role in the adsorption of Pb(II) onto the ACs surfaces at near neutral condition [73].

It should be noted that NaCl-Pb(II)/ACs system may not be controlled just by inner-sphere surface complexation. In the presence of NaCl, the adsorption of a part of Pb/(II) which probably adsorbed through outer-sphere complexation may be reduced due to the formation of Pb-Cl complex. This reduced Pb(II) adsorption rate may be compensated by precipitation of a part of Pb-Cl complexes. Overall, the negligible change of Pb(II) adsorption rate with increasing NaCl concentration is a resultant of all possible phenomena in NaCl-Pb(II)/ACs system.

4. Conclusion

In this study, date press cake, an agro-industrial waste, was converted into activated carbon through a two-stage procedure; carbonization and activation at 750°C with two different solid KOH:CM weight ratios (1:1 and 4:1). The adsorption of Pb(II) onto both ACs was well described by Elovich and pseudo-second order kinetic models, illustrating that the Pb(II) adsorption onto the ACs was predominantly a chemisorption process. Isotherm study illustrated multilayer adsorption of Pb(II) onto AC1 which took place on a heterogeneous surface. However, it was found that the Pb(II)/AC4 adsorption process occurred in a monomolecular layer with a homogenous distribution among the adsorption sites at different energies. AC4 showed higher S_{BET} and pore volume and contained more oxygen functional groups than AC1. Due to such properties, AC4 showed better performance for the adsorption of Pb(II) from aqueous solution. The adsorption system was not significantly influenced by ionic strength originated from NaCl. Therefore, the KOH-activated carbon derived from DPC could be successfully applied for the removal of Pb(II) even from saline aqueous solutions.

Acknowledgement

The authors acknowledge the financial support provided by the Vice Chancellor for Research in Hormozgan University of Medical Sciences (HUMS) (Grant No. 960327).

Conflict of interest

The authors of this article declare that they have no conflict of interests

References

[1] F. Fu, Q. Wang, Removal of heavy metal ions from wastewaters: a review, J. Environ. Manage., 92 (2011) 407–418.
[2] M. Boskabady, N. Marefati, T. Farkhondeh, F. Shakeri, A. Farshbaf, M.H. Boskabady, The effect of environmental lead exposure on human health and the contribution of inflammatory mechanisms, a review, Environ. Int., 120 (2018) 404–420.
[3] H. Bradl, Heavy metals in the environment: origin, interaction and remediation, Elsevier, London UK, 2005.
[4] J.S. Casas, J. Sordo, Lead: chemistry, analytical aspects, environmental impact and health effects, Elsevier, London UK, 2011.
[5] R.C. Gupta, Reproductive and developmental toxicology, Elsevier, London UK, 2011.
[6] M.A. Barakat, New trends in removing heavy metals from industrial wastewater, Arab. J. Chem., 4 (2011) 361–377.
[7] N. Ozbay, A.S. Yargic, Comparison of surface and structural properties of carbonaceous materials prepared by chemical activation of tomato paste waste: the effects of activator type and impregnation ratio, J. Appl. Chem., 2016 (2016) 1–10.
[8] S. Kumar, R. Sivaranjanee, A. Saravanan, Carbon sphere: Synthesis, characterization and elimination of toxic Cr(VI) ions from aquatic system, J. Ind. Eng. Chem., 60 (2018) 307–320.
[9] H. Tounsadi, A. Khalidi, M. Abdennouri, N. Barka, Activated carbon from Diplotaxis Harra biomass: Optimization of preparation conditions and heavy metal removal, J. Taiwan Inst. Chem. Eng., 59 (2016) 348–358.
[10] S. Das, S. Mishra, Box-Behnken statistical design to optimize preparation of activated carbon from Limonia acidissima shell with desirability approach, J. Environ. Chem. Eng., 5 (2017) 588–600.
[11] S. Pap, J. Radonić, S. Trifunović, D. Adamović, I. Mihajlović, M. Vojinović Miloradov, M. Turk Sekulić, Evaluation of the adsorption potential of eco-friendly activated carbon prepared from cherry kernels for the removal of Pb^{2+}, Cd^{2+} and Ni^{2+} from aqueous wastes, J. Environ. Manage., 184 (2016) 297–306.
[12] G.A. Adebisi, Z.Z. Chowdhury, P.A. Alaba, Equilibrium, kinetic, and thermodynamic studies of lead ion and zinc ion adsorption from aqueous solution onto activated carbon prepared from palm oil mill effluent, J. Clean. Prod., 148 (2017) 958–968.
[13] S.Z. Mohammadi, M.A. Karimi, S.N. Yazdy, T. Shamspur, H. Hamidian, Removal of Pb(II) ions and malachite green dye from wastewater by activated carbon produced from lemon peel, Quim. Nova., 37 (2014) 804–809.
[14] J.N. Sahu, J. Acharya, B.K. Sahoo, B.C. Meikap, Optimization of lead (II) sorption potential using developed activated carbon from tamarind wood with chemical activation by zinc chloride, Desal. Water Treat., 57 (2016) 2006–2017.

[15] M. Manjuladevi, R. Anitha, S. Manonmani, Kinetic study on adsorption of Cr(VI), Ni(II), Cd(II) and Pb(II) ions from aqueous solutions using activated carbon prepared from Cucumis melo peel, Appl. Water Sci., 8 (2018) 36.
[16] M. Chandrasekaran, A.H. Bahkali, Valorization of date palm (Phoenix dactylifera) fruit processing by-products and wastes using bioprocess technology – Review, Saudi J. Biol. Sci., 20 (2013) 105–120.
[17] Food and Agriculture Organization, FAOSTAT. Production; Crops, FAO. (2017). http://www.fao.org/faostat/en/#data/QC (accessed August 25, 2018).
[18] S. Ghnimi, S. Umer, A. Karim, A. Kamal-Eldin, Date fruit (Phoenix dactylifera L.): An underutilized food seeking industrial valorization, NFS J., 6 (2017) 1–10.
[19] S. Norouzi, M. Heidari, V. Alipour, O. Rahmanian, M. Fazlzadeh, F. Mohammadi-moghadam, H. Nourmoradi, B. Goudarzi, K. Dindarloo, Preparation, characterization and Cr(VI) adsorption evaluation of NaOH-activated carbon produced from date press cake; an agro-industrial waste, Bioresour. Technol., 258 (2018) 48–56.
[20] Y.B. Onundi, A.A. Mamun, M.F. Al Khatib, Y.M. Ahmed, Adsorption of copper, nickel and lead ions from synthetic semiconductor industrial wastewater by palm shell activated carbon, Int. J. Environ. Sci. Technol., 7 (2010) 751–758.
[21] J.R. García, U. Sedran, M.A.A. Zaini, Z.A. Zakaria, Preparation, characterization, and dye removal study of activated carbon prepared from palm kernel shell, Environ. Sci. Pollut. Res., 25 (2018) 5076–5085.
[22] E.-S.I. El-Shafey, H. Al-Lawati, A.S. Al-Sumri, Ciprofloxacin adsorption from aqueous solution onto chemically prepared carbon from date palm leaflets, J. Environ. Sci., 24 (2012) 1579–1586.
[23] E.-S.I. El-Shafey, S. Al-Busafi, H.A.J. Al-Lawati, A.S. Al-Shibli, Removal of Cu^{2+} and SO_4^{2-} from aqueous solutions on surface functionalized dehydrated carbon from date palm leaflets, J. Water Process Eng., 15 (2017) 62–71.
[24] K.Y. Foo, B.H. Hameed, Microwave-assisted preparation of oil palm fiber activated carbon for methylene blue adsorption, Chem. Eng. J., 166 (2011) 792–795.
[25] G.O. El-Sayed, Removal of methylene blue and crystal violet from aqueous solutions by palm kernel fiber, Desalination, 272 (2011) 225–232.
[26] Z. Heidarinejad, O. Rahmanian, M. Fazlzadeh, M. Heidari, Enhancement of methylene blue adsorption onto activated carbon prepared from date press cake by low frequency ultrasound, J. Mol. Liq., 264 (2018) 591–599.
[27] W.M. Daud, W.S. Ali, M.Z. Sulaiman, The effects of carbonization temperature on pore development in palm-shell-based activated carbon, Carbon, 38 (2000) 1925–1932.
[28] O. Pezoti, A.L. Cazetta, K.C. Bedin, L.S. Souza, A.C. Martins, T.L. Silva, O.O. Santos Júnior, J.V. Visentainer, V.C. Almeida, NaOH-activated carbon of high surface area produced from guava seeds as a high-efficiency adsorbent for amoxicillin removal: Kinetic, isotherm and thermodynamic studies, Chem. Eng. J., 288 (2016) 778–788.
[29] M. Thommes, K. Kaneko, A.V. Neimark, J.P. Olivier, F. Rodriguez-Reinoso, J. Rouquerol, K.S. Sing, Physisorption of gases, with special reference to the evaluation of surface area and pore size distribution (IUPAC Technical Report), Pure Appl. Chem., 87 (2015) 1051–1069.
[30] C. Miranda, J. Urresta, H. Cruchade, A. Tran, M. Benghalem, A. Astafan, P. Gaudin, T.J. Daou, A. Ramírez, Y. Pouilloux, A. Sachse, Exploring the impact of zeolite porous voids in liquid phase reactions: The case of glycerol etherification by tert-butyl alcohol, J. Catal., 365 (2018) 249–260.
[31] A.L. Cazetta, A.M.M. Vargas, E.M. Nogami, M.H. Kunita, M.R. Guilherme, A.C. Martins, T.L. Silva, J.C.G. Moraes, V.C. Almeida, NaOH-activated carbon of high surface area produced from coconut shell: Kinetics and equilibrium studies from the methylene blue adsorption, Chem. Eng. J., 174 (2011) 117–125.
[32] S.L. Goertzen, K.D. Thériault, A.M. Oickle, A.C. Tarasuk, H.A. Andreas, Standardization of the Boehm titration. Part I. CO_2 expulsion and endpoint determination, Carbon N. Y., 48 (2010) 1252–1261.
[33] H.P. Boehm, Some aspects of the surface chemistry of carbon blacks and other carbons, Carbon, 32 (1994) 759–769.
[34] W.-J. Liu, F.-X. Zeng, H. Jiang, X.-S. Zhang, Preparation of high adsorption capacity bio-chars from waste biomass, Bioresour. Technol., 102 (2011) 8247–8252.
[35] R.-L. Tseng, S.-K. Tseng, Pore structure and adsorption performance of the KOH-activated carbons prepared from corncob, J. Colloid Interface Sci., 287 (2005) 428–437.
[36] A.N. El-Hendawy, An insight into the KOH activation mechanism through the production of microporous activated carbon for the removal of Pb^{2+} cations, Appl. Surf. Sci., 255 (2009) 3723–3730.
[37] L. Muniandy, F. Adam, A.R. Mohamed, E.P. Ng, The synthesis and characterization of high purity mixed microporous/mesoporous activated carbon from rice husk using chemical activation with NaOH and KOH, Micropor. Mesopor. Mater., 197 (2014) 316–323.
[38] Q. Wang, X. Liang, W. Qiao, C. Liu, X. Liu, L. Zhan, L. Ling, Preparation of polystyrene-based activated carbon spheres with high surface area and their adsorption to dibenzothiophene, Fuel Process. Technol., 90 (2009) 381–387.
[39] A. Nieto-Márquez, A. Pinedo-Flores, G. Picasso, E. Atanes, R. Sun Kou, Selective adsorption of Pb^{2+}, Cr^{3+} and Cd^{2+} mixtures on activated carbons prepared from waste tires, J. Environ. Chem. Eng., 5 (2017) 1060–1067.
[40] T.L. Silva, A.L. Cazetta, P.S.C. Souza, T. Zhang, T. Asefa, V.C. Almeida, Mesoporous activated carbon fibers synthesized from denim fabric waste: Efficient adsorbents for removal of textile dye from aqueous solutions, J. Clean. Prod., 171 (2018) 482–490.
[41] S. Li, K. Han, J. Li, M. Li, C. Lu, Preparation and characterization of super activated carbon produced from gulfweed by KOH activation, Micropor. Mesopor. Mat., 243 (2017) 291–300.
[42] R. Khosravi, A. Zarei, M. Heidari, A. Ahmadfazeli, M. Vosughi, M. Fazlzadeh, Application of ZnO and TiO_2 nanoparticles coated onto montmorillonite in the presence of H_2O_2 for efficient removal of cephalexin from aqueous solutions, Korean J. Chem. Eng., (2018) 1000–1008.
[43] W.-H. Li, Q.-Y. Yue, B.-Y. Gao, Z.-H. Ma, Y.-J. Li, H.-X. Zhao, Preparation and utilization of sludge-based activated carbon for the adsorption of dyes from aqueous solutions, Chem. Eng. J., 171 (2011) 320–327.
[44] A. Kumar, H.M. Jena, Adsorption of Cr(VI) from aqueous solution by prepared high surface area activated carbon from Fox nutshell by chemical activation with H_3PO_4, J. Environ. Chem. Eng., 5 (2017) 2032–2041.
[45] R. Ahmad, S. Haseeb, Absorptive removal of Pb^{2+}, Cu^{2+} and Ni^{2+} from the aqueous solution by using groundnut husk modified with Guar Gum (GG): Kinetic and thermodynamic studies, Groundw. Sustain. Dev., 1 (2015) 41–49.
[46] T.M. Alslaibi, I. Abustan, M.A. Ahmad, A.A. Foul, Comparison of activated carbon prepared from olive stones by microwave and conventional heating for iron (II), lead (II), and copper (II) removal from synthetic wastewater, Environ. Prog. Sustain. Energy, 33 (2014) 1074–1085.
[47] A.M. Soliman, H.M. Elwy, T. Thiemann, Y. Majedi, F.T. Labata, N.A.F. Al-Rawashdeh, Removal of Pb(II) ions from aqueous solutions by sulphuric acid-treated palm tree leaves, J. Taiwan Inst. Chem. Eng., 58 (2016) 264–273.
[48] H. Liu, F. Li, L. Chen, J. Ding, M. Sun, H. Liu, F. Li, L. Chen, J. Ding, M. Sun, Adsorptive removal of Pb(II) ions with magnetic metal-organic frameworks from aqueous samples, Gen. Chem., 3 (2017) 134–139.
[49] L. Bo, Q. Li, Y. Wang, L. Gao, X. Hu, J. Yang, One-pot hydrothermal synthesis of thrust spherical Mg–Al layered double hydroxides/MnO_2 and adsorption for Pb(II) from aqueous solutions, J. Environ. Chem. Eng., 3 (2015) 1468–1475.
[50] M.H. Dehghani, A. Dehghan, A. Najafpoor, Removing Reactive Red 120 and 196 using chitosan/zeolite composite from aqueous solutions: Kinetics, isotherms, and process optimization, J. Ind. Eng. Chem., 51 (2017) 185–195.
[51] S. Lagergren, 'Zurtheorie der sogenannten adsorption gelosterstoffe', Kungliga svenskavetenskapsakademiens, Handlingar Band, 24 (1898) 1–39.

[52] Y.S. Ho, G. McKay, Pseudo-second order model for sorption processes, Process Biochem., 34 (1999) 451–465.
[53] S.Y. Elovich, O.G. Larinov, Theory of adsorption from solutions of non electrolytes on solid (I) equation adsorption from solutions and the analysis of its simplest form,(II) verification of the equation of adsorption isotherm from solutions, Izv. Akad. Nauk. SSSR, Otd. Khim. Nauk., 2 (1962) 209–216.
[54] S. Vilvanathan, S. Shanthakumar, Biosorption of Co(II) ions from aqueous solution using Chrysanthemum indicum: Kinetics, equilibrium and thermodynamics, Process Saf. Environ. Prot., 96 (2015) 98–110.
[55] Y. Yang, X. Yan, X. Hu, R. Feng, M. Zhou, W. Cui, Development of zeolitic imidazolate framework-67 functionalized Co-Al LDH for CO_2 adsorption, Colloids Surfaces A Physicochem, Eng. Asp., 552 (2018) 16–23.
[56] W.J. Weber, J.C. Morris, Kinetics of adsorption on carbon from solution, J. Sanit. Eng. Div., 89 (1963) 31–60.
[57] G.F. Malash, M.I. El-Khaiary, Piecewise linear regression: A statistical method for the analysis of experimental adsorption data by the intraparticle-diffusion models, Chem. Eng. J., 163 (2010) 256–263.
[58] G.E. Boyd, A.W. Adamson, L.S. Myers Jr, The exchange adsorption of ions from aqueous solutions by organic zeolites. II. Kinetics, J. Am. Chem. Soc., 69 (1947) 2836–2848.
[59] S. Wong, Y. Lee, N. Ngadi, I.M. Inuwa, N.B. Mohamed, Synthesis of activated carbon from spent tea leaves for aspirin removal, Chinese J. Chem. Eng., 26 (2018) 1003–1011.
[60] H.M.F. Freundlich, Over the adsorption in solution, J. Phys. Chem., 57 (1906) 385–471.
[61] I. Langmuir, The constitution and fundamental properties of solids and liquids. Part I. Solids, J. Am. Chem. Soc., 38 (1916) 2221–2295.
[62] O.J. Redlich, D.L. Peterson, A useful adsorption isotherm, J. Phys. Chem., 63 (1959) 1024–1026.
[63] M.I. Temkin, Kinetics of ammonia synthesis on promoted iron catalysts, Acta physiochim. URSS., 12 (1940) 327–356.
[64] K.Y. Foo, B.H. Hameed, Insights into the modeling of adsorption isotherm systems, Chem. Eng. J., 156 (2010) 2–10.
[65] S.Z. Mohammadi, M.A. Karimi, D. Afzali, F. Mansouri, Removal of Pb(II) from aqueous solutions using activated carbon from sea-buckthorn stones by chemical activation, Desalination, 262 (2010) 86–93.
[66] E.G. Lemraski, S. Sharafinia, Kinetics, equilibrium and thermodynamics studies of Pb^{2+} adsorption onto new activated carbon prepared from Persian mesquite grain, J. Mol. Liq., 219 (2016) 482–492.
[67] T.M. Alslaibi, I. Abustan, M.A. Ahmad, A.A. Foul, Application of response surface methodology (RSM) for optimization of Cu^{2+}, Cd^{2+}, Ni^{2+}, Pb^{2+}, Fe^{2+}, and Zn^{2+} removal from aqueous solution using microwaved olive stone activated carbon, J. Chem. Technol. Biotechnol., 88 (2013) 2141–2151.
[68] J. Sun, Z. Zhang, J. Ji, M. Dou, F. Wang, Removal of Cr^{6+} from wastewater via adsorption with high-specific-surface-area nitrogen-doped hierarchical porous carbon derived from silkworm cocoon, Appl. Surf. Sci., 405 (2017) 372–379.
[69] F. Boudrahem, F. Aissani-Benissad, H. Aït-Amar, Batch sorption dynamics and equilibrium for the removal of lead ions from aqueous phase using activated carbon developed from coffee residue activated with zinc chloride, J. Environ. Manage., 90 (2009) 3031–3039.
[70] M. Abdulkarim, F.A. Al-Rub, Adsorption of lead ions from aqueous solution onto activated carbon and chemically-modified activated carbon prepared from date pits, Adsorpt. Sci. Technol., 22 (2004) 119–134.
[71] Q. Fan, D. Shao, Y. Lu, W. Wu, X. Wang, Effect of pH, ionic strength, temperature and humic substances on the sorption of Ni(II) to Na–attapulgite, Chem. Eng. J., 150 (2009) 188–195.
[72] S. Goldberg, Inconsistency in the triple layer model description of ionic strength dependent boron adsorption, J. Colloid Interface Sci., 285 (2005) 509–517.
[73] Z. Liu, X. Zhong, Y. Wang, Z. Ding, C. Wang, G. Wang, S. Liao, An efficient adsorption of manganese oxides/activated carbon composite for lead(II) ions from aqueous solution, Arab. J. Sci. Eng., 43 (2018) 2155–2165.

Supplementary information

Table S1
General forms of the kinetic and isotherm models used in this study

Kinetic models	
Pseudo-first order	$q_t = q_e\left(1-e^{-k_1 t}\right); h_0 = k_1 q_e$
Pseudo-second order	$q_t = \frac{k_2 q_e^2 t}{1+k_2 q_e t}; h_0 = k_2 q_e^2$
Elovich	$q_t = \frac{1}{\beta}\ln\left(1+\alpha\beta t\right)$
Intraparticle diffusion	$q_t = k_{id}\sqrt{t} + C_i$
Boyd	$B_t = -\ln\left(1-\frac{q_t}{q_e}\right) - 0.4977$
Isotherm models	
Freundlich	$q_e = k_F C_e^{1/nf}$
Langmuir	$q_e = \frac{q_m k_L C_e}{1+k_L C_e}; R_L = \frac{1}{1+k_L C_e}$
Redlich-Peterson	$q_e = \frac{a_{RP} C_e}{1+b_{RP} C_e^g}$
Temkin	$q_e = \frac{RT}{b} ln\alpha + \frac{RT}{b}\ln C_e$

k_1 and k_2 = rate constants of the pseudo-first order and pseudo-second order models, respectively; h_0 = initial adsorption rate; α and β = Elovich constants; k_{id} and C_i = intraparticle diffusion constants, B_t = Boyd constant, k_F and n_f = Freundlich constants; q_m = maximum monolayer adsorption capacity; k_L = Langmuir constant; R_L = Langmuir separation factor; a_{RP} and b_{RP} = Redlich-Peterson constants; b = variation of the adsorption energy in Temkin model; R = universal gas constant (8.314 J mol^{-1} K^{-1}); T = absolute temperature (K).

Table S2
Error functions used in this study

Function name	Formula
The coefficient of determination (R^2)	$R^2 = \frac{\left(q_{meas}-\overline{q_{calc}}\right)^2}{\Sigma\left(q_{meas}-\overline{q_{calc}}\right)^2+\left(q_{meas}-\overline{q_{calc}}\right)^2}$
Average relative error (ARE)	$ARE = \frac{100}{n}\sum_{i=1}^{n}\left\|\frac{q_{meas}-q_{calc}}{q_{meas}}\right\|$

q_{meas} = measured adsorption capacity (mg g^{-1}); q_{calc} = calculated adsorption capacity (mg g^{-1}); $\overline{q_{calc}}$ = mean calculated adsorption capacity (mg g^{-1}); n = number of data points